Self-Assembled Three-Dimensional Nanocrown Array

Soongweon Hong,[†,∥] Taewook Kang,[‡,∥] Dukhyun Choi,[†,⊥] Yeonho Choi,[§,*] and Luke P. Lee[†,*]

[†]Biomolecular Nanotechnology Center, Berkeley Sensor and Actuator Center, Department of Bioengineering, University of California at Berkeley, Berkeley, California 94720, United States, [‡]Department of Chemical and Biomolecular Engineering, Sogang University, Seoul, 121-742, Korea, and [§]Department of Biomedical Engineering, Korea University, Seoul, 136-703, Korea. [⊥]Present address: Department of Mechanical Engineering, Kyung Hee University, Gyeonggi 446-701, Korea. [∥]These authors contributed equally to this work.

ABSTRACT

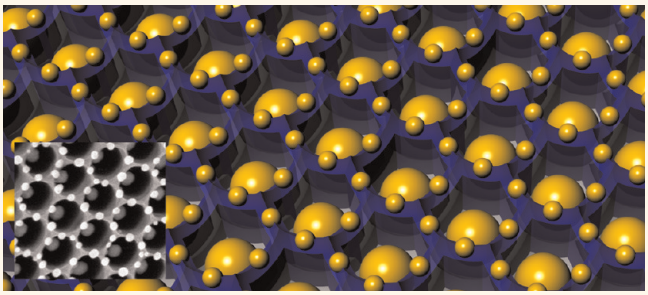

Although an ordered nanoplasmonic probe array will have a huge impact on light harvesting, selective frequency response (*i.e.*, nanoantenna), and quantitative molecular/cellular imaging, the realization of such an array is still limited by conventional techniques due to the serial processing or resolution limit by light diffraction. Here, we demonstrate a thermodynamically driven, self-assembled three-dimensional nanocrown array that consists of a core and six satellite gold nanoparticles (GNPs). Our ordered nanoprobe array is fabricated over a large area by thermal dewetting of thin gold film on hexagonally ordered porous anodic alumina (PAA). During thermal dewetting, the structural order of the PAA template dictates the periodic arrangement of gold nanoparticles, rendering the array of gold nanocrown. Because of its tunable size (*i.e.*, 50 nm core and 20 nm satellite GNPs), arrangement, and periodicity, the nanocrown array shows multiple optical resonance frequencies at visible wavelengths as well as angle-dependent optical properties.

KEYWORDS: self-assembled · dewetting · porous anodic alumina · plasmonic · nanoprobes

Owing to the great enhancement of light within the nanoscale and its induced unique optical characteristics, metallic nanostructures have received enormous interest in surface plasmon-based molecular detection methods including localized surface plasmon resonance (LSPR), surface-enhanced Raman spectroscopy (SERS), plasmon resonance energy transfer (PRET), and metal-enhanced fluorescence (MEF).[1−7] For sensitivity and selectivity, significant advances have already been accomplished, such as single-molecule detection and tunability of nanoantenna resonance frequency, respectively.[7] However, the fluctuation of the amplitude in the sensing signal has been pointed out as a major drawback in plasmonic-based molecular detection. Although an ordered nanoplasmonic array over a large area has received great interest as a solution for quantification, reproducibility, and nanoscale spatial resolution, it is still a challenge to obtain an ordered metallic nanostructure array by conventional fabrication technologies. Here, we demonstrate a three-dimensional (3-D) ordered plasmonic nanostructure of the nanocrown array. Each unit of the array consists of a centric sphere particle (*ca.* 50 nm diameter) and six surrounding satellite particles (*ca.* 20 nm diameter) with a unique two-layer arrangement (Figure 1). The nanocrown array is fabricated easily in a large area by a thermodynamically driven self-assembled process (by the deposition of a thin gold film onto preordered dielectric nanohole patterns, followed by thermal annealing). This unique plasmonic substrate can provide several benefits in optical applications by combining advantages of conventional nanofabrication methods. First, a nanocrown is optically tunable. As reported previously, most of the plasmonic nanostructures have been targeted to have a resonance wavelength in the range from visible to near-infrared (NIR) due to the penetration depth, excitation light source capability, and spectral change detectability.[1−3,8] In order to satisfy these constrains, 10−100 nm metallic nanostructures are required. However, some parallel fabrication techniques, such as block copolymer lithography, ordered template-based nanofabrication, and self-assembly methods, are limited in optical tunability despite successful small size patterns in a large area.[9−12] Since the nanocrown consists of a 50 nm core nanosphere on the bottom and six 20 nm satellite nanoparticles on a higher-plane rim, various resonance frequencies within the

* Address correspondence to yeonhochoi@korea.ac.kr, lplee@berkeley.edu.

Received for review December 19, 2011 and accepted June 5, 2012.

Published online June 05, 2012
10.1021/nn204967k

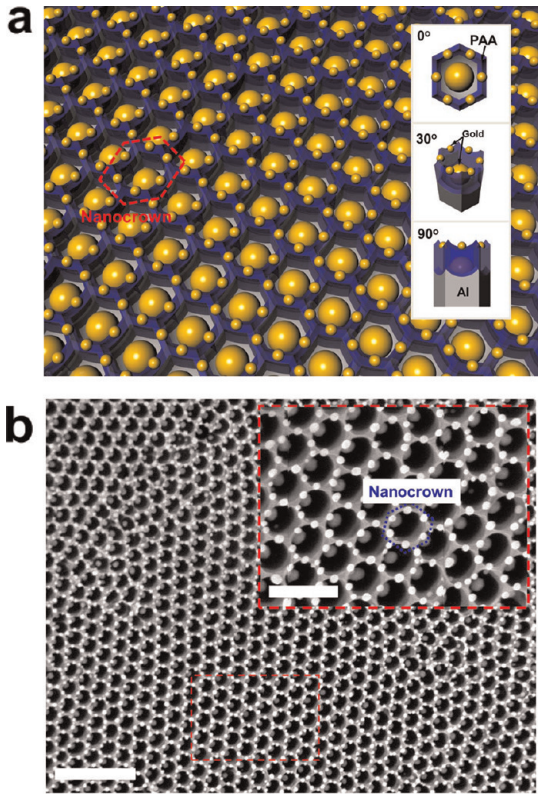

Figure 1. Three-dimensional nanoplasmonic probe array: nanocrown. (a) Schematic diagram for label-free molecular detection using the nanocrown. The inset shows the schematic representation (with different angles) of the nanocrown, showing that a single nanocrown consists of larger spherical gold nanoparticles at the center and six smaller satellite particles around the hexagon. (b) Secondary electron microscopy (SEM) image of a nanocrown array from pure porous anodic alumina (PAA) (80 nm diameter and 500 nm PAA thickness) with a 10 nm gold thin layer on top after annealing at 550 °C for 3 h. The magnified SEM image of selected area (red-dotted box) is shown in the inset. The scale bars in the main panels and inset SEM images represent 500 and 200 nm, respectively.

visible range can be obtained by controlling the distance between the center and satellite particles. Moreover, a double-layered array of nanoparticles in the nanocrown can increase spatial density, which will induce significant improvement of the spatial resolution. On the other hand, previously described methods fabricate the nanostructure in a single plane so that its density is inherently limited. Lastly, in analogy to three-dimensional photonic crystals, the nanocrown provides angle dependency of far-field optical properties. Therefore, it can be used as a multichannel nanoantenna which has different resonance frequencies as a function of excitation angle.

RESULTS AND DISCUSSION

As shown in Figure 2, high purity aluminum plates are electrochemically anodized to get porous anodic alumina (PAA), a hexagonally arrayed uniform size nanohole substrate with a spatial period of 100 nm. Additional chemical etching on aluminum oxide

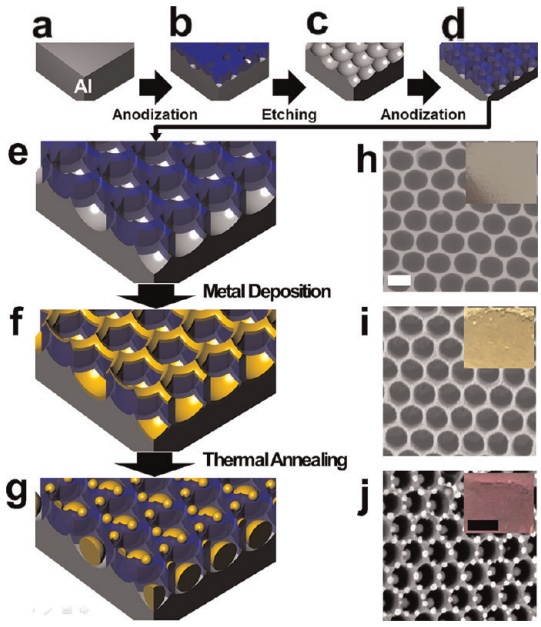

Figure 2. Fabrication steps of a nanocrown array: (a) pure aluminum sample, (b) first anodized PAA, (c) self-assembled aluminum after removing the PAA layer by wet-etching, (d) second anodized PAA, (e) pore size widened PAA, (f) Au-coated PAA, (g) self-assembled nanocrown array after annealing (550 °C for 3 h), (h–j) corresponding SEM images of (e–g), respectively. Insets show the bright-field optical images. The scale bars in the main SEM and inset images represent 100 nm and 1 cm, respectively.

modulates diameter of the nanohole from 30 to 80 nm. Here, the final PAA configuration in this study is the nanohole arrays surrounded by 20 nm thin nanowalls, 100 nm center-to-center distance, and the various depths by anodization time (*e.g.*, 100, 200, 500, and 1000 nm). On top of these PAA substrates, thin gold films are evaporated and the deposited gold layer transforms into an array of gold nanospheres by a thermal dewetting process (550 °C for 3 h, N_2 environment). In general, a dewetting process starts from rupturing a thin liquid film to form holes, which arises from surface tension stresses caused by high temperature and molecular interaction change between the substrate and the film. As a next step, the holes grow to form a polygonal network of straight liquid rims. It leads to accumulation of the materials along the perimeter of the holes. Eventually, droplets are formed *via* a Rayleigh instability which is represented by the characteristic wavelength ($\lambda_m \propto h^2$, where h is the film thickness).[13−22] Since preparation of the PAA substrate, metal film deposit, and dewetting can take place over a large area, it is a simple and effective self-organization method to fabricate metal nanostructures. However, unlike spinodal dewetting (*i.e.*, hole formation by a linear surface instability), heterogeneous dewetting (*i.e.*, hole nucleation on defects) during film rupture leads to making randomly located droplets, which results in metal islands with the broad distributions of size and space. Therefore, the ordered template is used as a substrate, in order to minimize heterogeneous dewetting

and fabricate a nanoplasmonic probe array with uniformity over a large area. Consequently, we could achieve the fabrication of a large-area array having one core nanosphere and six satellite particles on bottom and top, respectively (Supporting Information Figure S1).

In order to find the optimum experimental conditions for a highly uniform nanocrown array, we first investigated the nanohole size effect. When the diameter of the nanohole was 30 nm, the size and spacing of nanoparticles are not uniform and regular (Supporting Information Figure S2a). On the other hand, when its diameter increased to 80 nm, nanoparticle sizes are clearly divided into two groups, which are 50 and 20 nm in the two different height layers (Supporting Information Figure S2b). Since isolated nanohole areas were growing and connected wall areas decreased with increasing nanoholes, we believe that heterogeneous dewetting was significantly decreased with increasing hole size, and it resulted in a uniform nanoparticle array. Next, we investigated the effect of the gold film thickness. When it was 10 nm, a perfectly ordered nanocrown array was obtained after thermal annealing. However, in the case of 20 and 30 nm thickness, clear gold nanospheres were not formed on the PAA template due to the excessive quantity of gold (Supporting Information Figures S3 and S4). As the third experimental condition, we changed PAA depths from 100 to 1000 nm. In the case of the 1000 nm sample, the centric nanospheres in the nanoholes were not formed because the high aspect ratio of the hole makes it difficult for gold to be deposited on the bottom; instead, 5−10 nm size of nanoparticles was observed at the side walls (Supporting Information Figure S5). Lastly, the annealing temperature was controlled in the range between 400 and 600 °C. When the temperature was lower than 500 °C, the annealing process did not take place. On the other hand, the PAA-based template completely collapsed after thermal treatment when the temperature was 600 °C (data not shown).

As shown in the insets of Figure 2i,j, surface colors are dramatically changed after thermal annealing due to the uniformity of the size and spacing of gold nanoparticles in the nanocrown. In order to quantify the change of optical properties, they were measured as a function of PAA heights (*i.e.*, the distance between core and satellite nanoparticles) and the excitation angle of the light source. Since the bottom layer of the nanocrown (*i.e.*, aluminum) was a perfectly reflectional surface in the range of visible wavelengths, optical reflection was measured, and the results were recalculated to show the absorbance that is the sum of optical absorption and scattering (Supporting Information Figure S6). Figure 3 shows the representative extinction profiles with respect to PAA heights for the normal direction of light excitation (*i.e.*, $\theta = 0$). As height increased from 100 to 500 nm, double

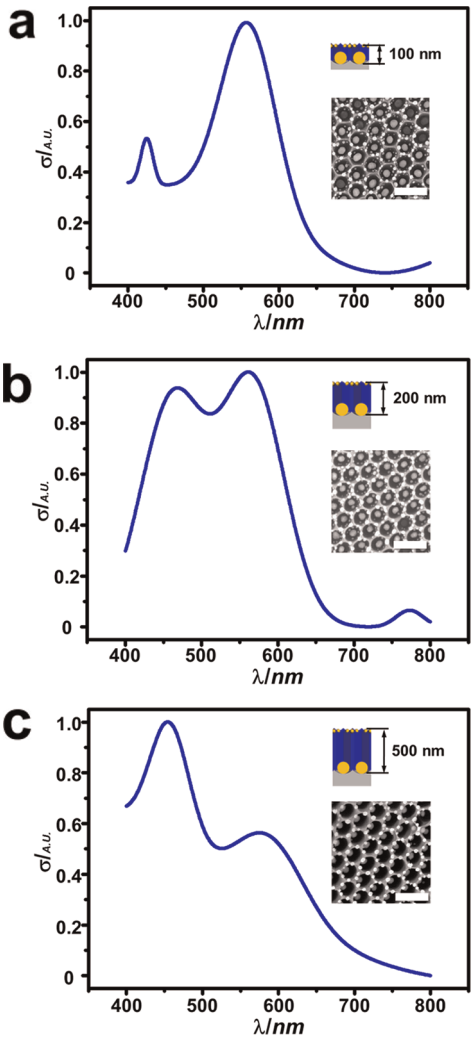

Figure 3. Extinction profile of the nanocrown for normal excitation as a function of dielectric layer (*i.e.*, PAA) depths: (a) 100 nm, (b) 200 nm, and (c) 500 nm. The scale bars in the insets are 200 nm.

resonance frequencies were observed; the first resonance peak was always shown between 430 and 460 nm, and the magnitude and position of the resonance peaks slightly increased or remained the same. In addition, the second peak position was almost fixed near 560 nm, and the amplitude consistently decreased with increasing heights. In the case of 1000 nm, four multiple resonance peaks were observed at 415, 450, 530, and 650 nm (Supporting Information Figure S7). We believe that the core nanoparticle in the nanocrowns is the origin of the second peak because the resonance frequency of the 50 nm gold nanosphere is well matched with its peak position. Moreover, as the height of PAA increases, the distance between the core and satellite gold nanosphere increases and it results in the amplitude and position of the first resonance frequency. However, as shown in Figure S5b, multiple gold nanoparticles on side walls were created and core nanoparticles in the center were not generated in the 1000 nm PAA case.

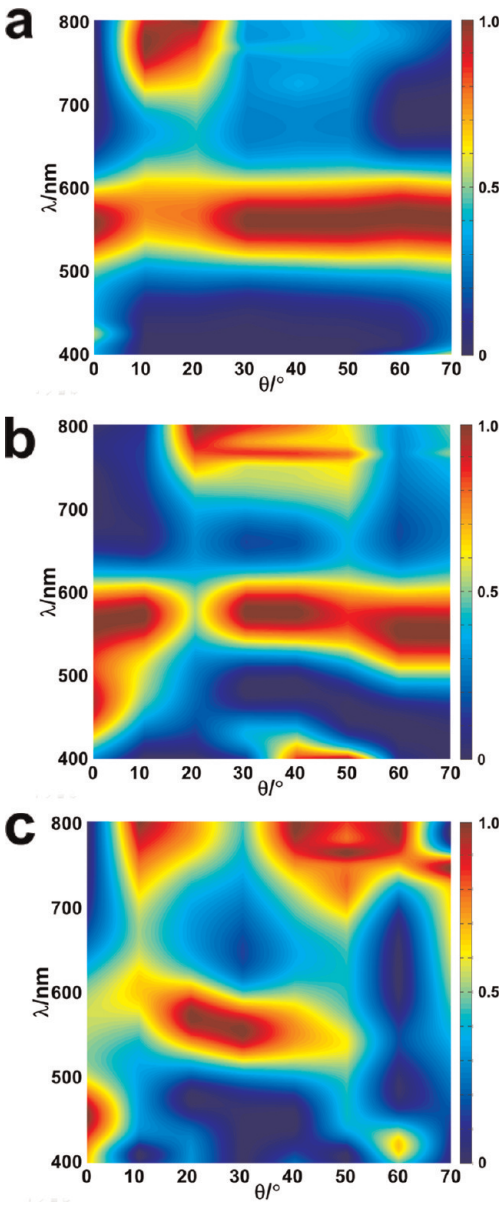

Figure 4. Angle-dependent extinction profiles of nanocrowns. The height of PAA is (a) 100 nm, (b) 200 nm, and (c) 500 nm.

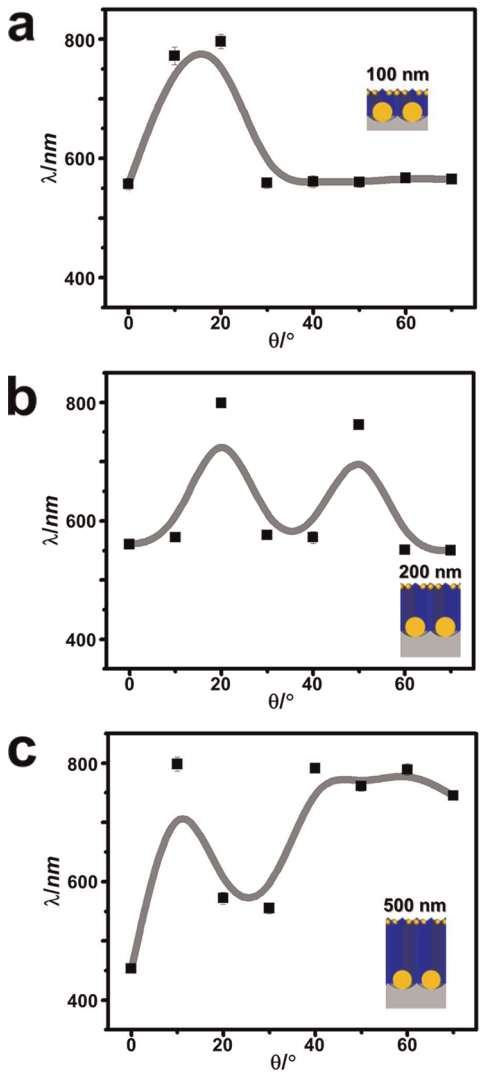

Figure 5. Angle-dependent extinction profile changes. Three different PAA heights, (a) 100, (b) 200, and (c) 500 nm, are fabricated and measured for the optical characterization.

It is considered that the relatively long side wall acts as an obstacle for gold atoms to reach the bottom of PAA during deposition. As a result, spherical nanoparticles are generated on the side wall while the thermal annealing process is performed. Different sizes of gold nanoparticles and their interaction in the 1000 nm sample are believed to generate two different resonances at 530 and 650 nm from 560 nm, whereas increased resonance peaks at 400−500 nm can be attributed to the optical properties of the 1000 nm deep cylindrical photonic structures.

Next, we investigated the angle-dependent optical properties by changing the excitation angle of the light source from 0 to 70° (see Supporting Information Figure S6). As the excitation angle increases, extinction profiles dramatically change compared to the normal excitation results (Figure 4). In detail, the change of resonance wavelength and those extinction amplitudes becomes sensitive as a function of excitation angle and PAA height, as shown in Figure 5. All nanocrown samples show significant red shift of the resonance peak (*i.e.*, second peak in normal excitation) from 500 to 800 nm as the excitation angle increases and returns to the similar resonance wavelength of normal excitation at the angle of 30°. Higher angle excitation than 30° generated more dramatic change in the excitation spectra, which was strongly dependent on PAA height. For example, the peak position was maintained in the 100 nm case, but a 200 nm sample shows a red shift and a constant resonance peak. Since the distance between core and satellite gold nanoparticles increases with an increase of PAA height and the excitation angle, the order of the change dramatically increases with PAA height.

In order to check the possibility as plasmonic-based molecular probes, SERS-based molecular sensing was performed. Nanocrowns show consistent and reliable SERS spectra of the target molecules (Supporting Information Figure S8).

CONCLUSION

In conclusion, we have demonstrated a self-assembled three-dimensional nanoplasmonic probe array, named nanocrown, by using a simple thermal treatment. The nanocrown consists of a 50 nm core and six 20 nm satellite gold nanoparticles on an ordered porous anodic alumina (PAA) template and can be formed by a thermally induced dewetting process. On the basis of the advantage of the dewetting, the nanocrown can be fabricated without the limitation of the area and the PAA-based ordered template makes the nanocrown show a perfectly ordered nanoplasmonic pattern by minimizing the heterogeneous dewetting, which is the major reason to generate the randomly distributed nanoparticles. Moreover, the three-dimensionally located nanocrown successfully demonstrates angle-dependent optical properties and can be controlled by adjusting the distance between the core and satellite gold nanoparticles. Owing to large-area fabrication, self-ordered array, optical tunability in visible wavelengths, and angle-dependent resonance frequencies, we believe that the nanocrown will have an impact on the field of molecular sensing for quantitative measurement and multiplexing with high spatial resolution, sensitivity, and selectivity.

MATERIALS AND METHODS

Preparation of the PAA Template. A pure aluminum sheet of 99.999% (1 mm thickness) was electropolished to remove surface irregularities. After washing the surface, electrochemical anodization was conducted by using 0.3 M oxalic acid solution overnight. After this first anodization, the aluminum oxide layer was removed to expose a uniform dimple aluminum surface by the treatment with the mixture of 1.8% chromic acid and 6% phosphoric acid at 65 °C for 6 h. Then second anodization was applied under the same condition as the first anodization with varying treatment times to control the depth of the aluminum oxide nanopore (about 100 nm depth per 1 min). To widen the nanopore diameter of PAA from 30 to 80 nm, PAA was treated with phosphoric acid of 0.1 M for several hours.

Fabrication of the Nanocrown. The evaporation of gold film was performed using an e-beam evaporator (Edwards EB3). The thickness was controlled by the evaporation time. Three different thicknesses (10, 20, and 30 nm) of gold film were deposited. Thermal annealing for the dewetting process was done in a tube-type furnace at the condition of 550 °C for 3 h under N_2 environment. Note that the dewetting cannot be uniform when the gold-coated PAA is slightly tilted.

Extinction Measurements. Owing to the opaqueness of the nanocrown, reflectance-based extinction was measured. White light (DT 100CE, Analytical Instrument System Inc.) was illuminated, and the reflected response was collected through an optical fiber and sent to a spectrometer (Ocean Optics Inc. SD2000). For the angle-dependent optical properties, the optical fibers were fixed and maintained the same angle for the excitation and the measurement by a holder (see Supporting Information Figure S6).

Conflict of Interest: The authors declare no competing financial interest.

Acknowledgment. This work is supported by a grant of the Korea Healthcare Technology R&D Project, Ministry of Health & Welfare, Republic of Korea (Grant No. A103001), and the Basic Science Program through the National Research Foundation of Korea (NRF) funded by the Ministry of Education, Science, and Technology (Grant No. 2011-0025895).

Supporting Information Available: Additional figures. This material is available free of charge *via* the Internet at http://pubs.acs.org.

REFERENCES AND NOTES

1. Halas, N. J. Plasmonics: An Emerging Field Fostered by Nano Letters. *Nano Lett.* **2010**, *10*, 3816–3822.
2. Stewart, M. E.; Christopher, R. A.; Thompson, L. B.; Maria, J.; Gray, S. K.; Rogers, J. A.; Nuzzo, R. G. Nanostructured Plasmonic Sensors. *Chem. Rev.* **2008**, *108*, 494–521.
3. Stiles, P. L.; Dieringer, J. A.; Shah, N. C.; Van Duyne, R. P. Surface-Enhanced Raman Spectroscopy. *Annu. Rev. Anal. Chem.* **2008**, *1*, 601–626.
4. Khoury, C. G.; Norton, S. J.; Vo-Dinh, T. Plasmonics of 3-D Nanoshell Dimers Using Multipole Expansion and Finite Element Method. *ACS Nano* **2009**, *3*, 2776–2788.
5. Choi, Y.; Park, Y.; Kang, T.; Lee, L. P. Selective and Sensitive Detection of Metal Ions by Plasmonic Resonance Energy Transfer-Based Nanospectroscopy. *Nat. Nanotechnol.* **2009**, *4*, 742–746.
6. Aouani, H.; Wenger, J.; Gerard, D.; Rigneault, H.; Devaux, E.; Ebbesen, T. W.; Mahdavi, F.; Xu, T.; Blair, S. Crucial Role of the Adhesion Layer on the Plasmonic Fluorescence Enhancement. *ACS Nano* **2009**, *3*, 2043–2048.
7. Emory, S. R.; Nie, S. Probing Single Molecules and Single Nanoparticles by Surface-Enhanced Raman Scattering. *Science* **1997**, *275*, 1102–1106.
8. Lal, S.; Link, S.; Halas, N. J. Nano-optics from Sensing to Waveguiding. *Nat. Photonics* **2007**, *1*, 641–648.
9. Lee, W.; Han, H.; Lotnyk, A.; Schubert, M. A.; Senz, S.; Alexe, M.; Hesse, D.; Baik, S.; Gosele, U. Individually Addressable Epitaxial Ferroelectric Nanocapacitor Arrays with near Tb inch^{-2} Density. *Nat. Nanotechnol.* **2008**, *3*, 402–407.
10. Kempa, K.; Kimball, B.; Rybczynski, J.; Huang, Z. P.; Wu, P. F.; Steeves, D.; Sennett, M.; Giersig, M.; Rao, D. V. G. L. N.; Carnahan, D. L.; *et al.* Photonic Crystals Based on Periodic Arrays of Aligned Carbon Nanotubes. *Nano Lett.* **2003**, *3*, 13–18.
11. Li, Y.; Meng, W.; Zhang, L. D.; Phillipp, F. Ordered Semiconductor ZnO Nanowire Arrays and Their Photoluminescence Properties. *Appl. Phys. Lett.* **2000**, *76*, 2011–2013.
12. Henzie, J.; Lee, M. H.; Odom, T. W. Multiscale Patterning of Plasmonic Metamaterials. *Nat. Nanotechnol.* **2007**, *2*, 549–554.
13. Herminghaus, S.; Jacobs, K.; Mecke, K.; Bischof, J.; Fery, A.; Ibn-Elhaj, M.; Schlagowski, S. Spinodal Dewetting in Liquid Crystal and Liquid Metal Films. *Science* **1998**, *282*, 916–919.
14. Thiele, U.; Mertig, M.; Pompe, W. Dewetting of an Evaporating Thin Liquid Film; Heterogeneous Nucleation and Surface Instability. *Phys. Rev. Lett.* **1998**, *80*, 2869–2872.
15. Bischof, J.; Scherer, D.; Herminghaus, S.; Leiderer, P. Dewetting Modes of Thin Metallic Films: Nucleation of Holes and Spinodal Dewetting. *Phys. Rev. Lett.* **1996**, *77*, 1536–1539.
16. Kargupta, K.; Sharma, A. Templating of Thin Films Induced by Dewetting on Patterned Surfaces. *Phys. Rev. Lett.* **2001**, *86*, 4536–4539.

17. Becker, J.; Grun, G.; Seemann, R.; Mantz, H.; Jacobs, K.; Mecke, K. R.; Blossey, R. Complex Dewetting Scenarios Captured by Thin-Film Models. *Nat. Mater.* **2002**, *2*, 59–63.
18. Zhao, K.; Averback, R. S.; Cahill, D. G. Patterning of Metal Nanowires by Directed Ion-Induced Dewetting. *Appl. Phys. Lett.* **2006**, *89*, 053103.
19. Muller, C. M.; Mornaghini, F. C. F.; Spolenak, R. Ordered Arrays of Faceted Gold Nanoparticles Obtained by Dewetting and Nanosphere Lithography. *Nanotechnology* **2008**, *19*, 485306.
20. Giermann, A. L.; Thompson, C. V. Solid-State Dewetting for Ordered Arrays of Crystallographically Oriented Metal Particles. *Appl. Phys. Lett.* **2005**, *86*, 121903.
21. Yang, S. K.; Xu, F.; Ostendorp, S.; Wilde, G.; Zhao, H. P.; Lei, Y. Template-Confined Dewetting Process to Surface Nanopartterns. *Adv. Funct. Mater.* **2011**, *21*, 2446.
22. Yang, S. K.; Cao, B. Q.; Kong, L. C.; Wang, Z. Y. Templated-Directed Dewetting of a Gold Membrane to Fabricate Highly SERS-Active Substrates. *J. Mater. Chem.* **2011**, *21*, 14031.